Powder Technology 445 (2024) 120100

Contents lists available at ScienceDirect

Powder Technology

journal homepage: www.journals.elsevier.com/powder-technology

Influence of rotations in energy transfer of a particle colliding on a flat surface

F.E. Fernández [a], M.A. Aguirre [b,*], R.G. Martino [c], A. Boschan [b], M.F. Piva [a]

[a] Grupo de Medios Porosos, Fac. de Ingeniería, Universidad de Buenos Aires, Paseo Colón 850, (C1063ACV) Buenos Aires, Argentina
[b] Grupo de Medios Porosos, Fac. de Ingeniería, Universidad de Buenos Aires, CONICET, Paseo Colón 850, (C1063ACV) Buenos Aires, Argentina
[c] IDIT - CONICET - Universidad Nacional de Córdoba, Av. Velez Sarsfield 1611, (5000) Córdoba, Argentina

HIGHLIGHTS

- Dependent on impact velocity, some collisions lead to a coefficient of restitution $\epsilon > 1$.
- $\epsilon > 1$ mostly appears when rotational energy is transferred to motion normal to impact.
- N-faceted particles with $N \leq 15$ can induce more notorious rotations.

GRAPHICAL ABSTRACT

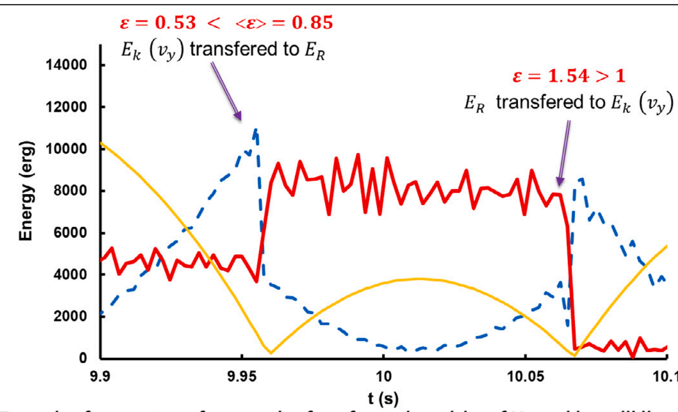

Example of energy transfer occurring for a faceted particles of N = 9 sides colliding with a flat surface.

$E_k\ (v_y)$: *Translational kinetic energy associated with the vertical motion*
E_R : *Rotational kinetic energy*
E_P : *Potential energy*

ARTICLE INFO

Keywords:
Coefficient of restitution
Energy dissipation
Particle collision

ABSTRACT

To understand the influence of rotations on the dissipation of energy in the interaction between a grain and its environment, we investigate the relaxation process of a single particle bouncing on a flat horizontal surface. For this purpose, faceted particles were used to promote the appearance of rotations in each bounce. The evolution of potential, translational and rotational kinetic energies was analyzed during the whole relaxation process, particularly focusing on the behavior just before and after each collision. The rebounding action of an individual grain results in energy dissipation commonly quantified by ϵ, the coefficient of restitution. This coefficient is defined as the ratio of the normal velocity component prior to impact (V_n) to the corresponding component immediately following the collision (V_n'), i.e. related to translational kinetic energy associated with motion in the normal direction. We identify a critical impact velocity below which, in certain collisions, $\epsilon > 1$. This phenomenon can be attributed to stored rotational kinetic energy which is transferred to translational kinetic energy during the collision, thereby increasing the normal velocity V_n' and resulting in the observed high values of ϵ.

* Corresponding author.
E-mail address: maaguir@fi.uba.ar (M.A. Aguirre).

https://doi.org/10.1016/j.powtec.2024.120100
Received 12 May 2024; Received in revised form 12 July 2024; Accepted 16 July 2024
Available online 19 July 2024

1. Introduction and background

The objective of this study is to examine the role of rotations in the dissipation of energy as a grain interacts with its surroundings while relaxing to equilibrium. In particular, this investigation is significant to understand how highly dissipative systems, such as those constituted by grains, exchange energy and achieve equilibrium which is crucial to understand stability problems of granular systems, such as the triggering and arrest of avalanches [1–4], sediment or particle transport down on hillslopes [5,6], as well as many processes in bioingeenering, mining, food and pharmaceutical industries [7–10].

The dissipation effects resulting from collisions are typically quantified by ϵ, the coefficient of restitution, which relies on various factors including material characteristics, surface roughness, body shape, temperature, environment and impact velocity [11–19].

This coefficient ϵ is an important collision parameter used to describe and characterize particle impact features (impact forces, particles deformation, time of deformation and others) that, are needed in the mathematical modeling and simulation [15,20–23], e.g discrete element method (DEM) and event driven methods, of processes and phenomena involving the flow and stability of non consolidate materials which allows to design equipment for manufacturing and handling granular material in different industries, e.g. in biomass fragmentation, in gravel cushions to avoid hazards in open-pit mines, seeders and for transportation of pharmaceutical tablets among many others [7–9,18, 23].

For a particle colliding with a non moving surface, this coefficient is determined as the ratio of the normal velocity component immediately after collision (V_{out}) to the one just before impact (V_{in}) [11–13]. It is expected that, due to dissipation in the collision, $\epsilon \leq 1$ and eventually, for perfectly elastic collision $\epsilon = 1$.

In many scenarios, the shape of grains or experimental setups do not permit the detection and measurement of impact points and rotations. Consequently, V_{in} and V_{out} are typically approximated using V_n and V_n', the normal component of the translational velocities of the particle's geometric center before and after impact, respectively. Therefore, the coefficient of restitution is usually defined as follows:

$$\epsilon = -\frac{V_n'}{V_n} \tag{1}$$

Note that values of ϵ, as defined by Eq. (1), do not considered motions in other degrees of freedoms beside motion in the normal direction. Therefore, in the following, we examine the behavior of a particle as it returns to its resting state after successive bounces on a flat surface to investigate how ϵ values are influenced by rotations and tangential motions not considered by its definition.

In this work, we analyzed the behavior of N-faceted particles, where $N = 3, 4, 5, 6, 7, 8, 9, 10, 15$ and ∞, i.e. a disk. For some values of N the rotation effects disregarded by Eq. (1) lead to some collisions with $\epsilon > 1$. This observation is analyzed in terms of energy stored in other degrees of freedom and transferred to kinetic energy, leading to an increase in normal velocity after impact, V_n'. To achieve this, the energy transfer among the different degrees of freedom was studied and therefore, we analyzed the evolution of kinetic, potential, and rotational energy throughout the relaxation process and immediately before and after each collision. Additionally, we find it pertinent to examine another coefficient that encompasses total energy.

$$\epsilon_E = \frac{E'}{E} \tag{2}$$

where E and E' are the particle total energy just before and after the collision, respectively.

The total energy of the particle accounts for potential energy, kinetic translational energy associated with horizontal and vertical motion, and kinetic rotational energy. Although this coefficient offers greater accuracy than ϵ, it is challenging to measure it in $3D$ situations.

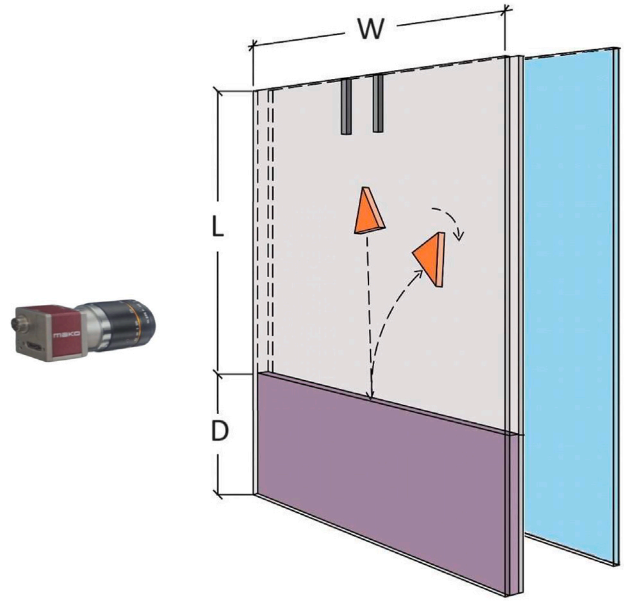

Fig. 1. Experimental setup schematic: The cell, made up of two glasses with a plexiglass base, is backlit by a light panel. For clarity, the aluminum frame supporting the cell and the tripod holding the camera are omitted.

In previous experiments, the coefficient of restitution (ϵ) for the bouncing of steel spheres on a steel flat surface was indirectly derived from the time between successive collisions and a significant dispersion in ϵ was observed [11]. Montaine et al. suggest that this dispersion arises from the assumption in the experimental methodology that the particle is point-like and that its energy comprises only potential and translational energy, disregarding any rotational energy effects. They argue that micro-roughness on sphere and platform surfaces could induce torques due to misalignment between the line joining the sphere-surface contact point and the sphere's center relative to the axis of gravity, leading to rotations that redistribute energy, not accounted for in the mentioned coefficient. Also, both Montaine et al. [11] and King et al. [12] observed that the dispersion for the coefficient of restitution diminishes as the initial impact velocity increases.

2. Experimental set-up and procedure

As mentioned in Section 1, Montaine et al. [11] observed a large dispersion in the coefficient of restitution obtained for a steel sphere impacting a flat surface. They conjecture that this is due to the reciprocal transfers between translational kinetic and rotational kinetic energy not being taken into account in the experimental methodology designed to obtain this coefficient. To study these energy transfers, a quasi-two-dimensional experiment was designed, in which the particles move between two proximate transparent vertical flat glasses. Thus, movement is confined to a vertical plane enabling the dynamics to be captured with a single camera (Fig. 1).

The experimental protocol involves releasing a particle into a vertical cell that consists of two glass pieces fixed to an aluminum frame. The cell has length $L = (21.5 \pm 0.1)$ cm and a width $W = (30.0 \pm 0.1)$ cm, separated by a gap of $W_g = (4.2 \pm 0.1)$ mm, slightly wider than the particle's width. The particle is positioned with its center aligned with the upper edge of the cell, a distance $H_o = (21.5 \pm 0.1)$ cm above the base and is released without any rotational motion from this initial height. Upon release, the particle collides with a flat plexiglass surface, of height $D = (7.5 \pm 0.1)$ cm and thickness 5 cm, and subsequently rebounds until it comes to a rest. The flat plexiglass is glued to one of the glasses. Thus, the total mass of the set is much greater than the mass of the particles, so its inertia is considered infinite.

Table 1
Radius R_N of the circle needed to circumscribed each faceted particles in order to ensure that they share the same area A and mass m. Error for all values of R_N is 0.1 mm.

N	3	4	5	6	7	8	9	10	15	∞
R_N (mm)	23.3	18.8	17.2	16.5	16.1	15.8	15.6	15.5	15.2	15.1

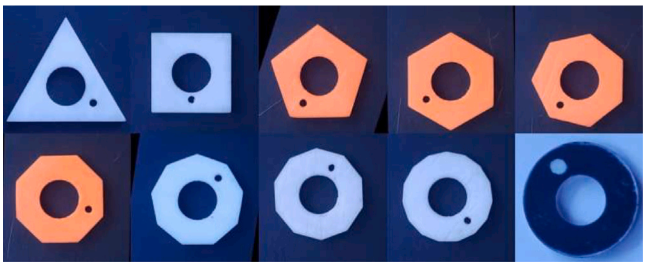

Fig. 2. Image of N faceted particles. Top row: $N = 3, 4, 5, 6, 7$. Bottom row: $N = 8, 9, 10, 15$ and ∞, i.e. a disk.

The system is backlit by a uniform light panel. A camera positioned in front of the cell, centered on the area of interest, records the images. Distortions at the edges of the visual field are minimal and can be disregarded. In each case, the trajectory of each particle (some examples can be found in [24]) is measured allowing to obtain:

- the velocity during the whole trajectory and, in particular, before and after each impact,
- the potential, translational and rotational kinetic energies and, consequently, the total energy. These energies will be obtained during the whole trajectory and in particular before and after each impact.

In order to promote the appearance of rotations after collisions the relaxation process of faceted flat particles was analyzed. The flat N-faceted particles with $N = 3, 4, 5, 6, 7, 8, 9, 10, 15$ and ∞, i.e. a disk, were 3D printed (3D printer CreateBOT-MID) with polylactide (PLA) which is a common thermoplastic frequently used to print rigid particles due to its versatility and resistance [25] (Fig. 2). Particle with more than 15 edges were not used because accuracy is not guaranty due to the 3D printer's resolution of the step angle of its stepper motor. Similar to particles used in a previous study [1], these N-faceted particles also have a centered circular orifice of radius $r = (0.75 \pm 0.1)$ cm which is used to easily track the faceted particle's center of mass position, i.e. the center of mass of the centered circular orifice. Each particle has a thickness of 4 mm and, near the border, they have a small orifice (less than 2 mm of diameter) that allows to trace rotations with respect to their center of mass. The small hole dimensions ensures that for each particle the position of its center of mass can be assumed to coincide with its geometrical center, i.e. the center of mass of the centered circular orifice. Each N-faceted particle can be exactly contained in a circle of radius R_N (Table 1) whose values are determined to ensure that all particles share the same area $A = (7.1 \pm 0.1)$ cm^2, i.e. same mass $m = (2.7 \pm 0.5)$ g.

Throughout the experiment, a Mako U-051B camera records the process at a sampling rate of 391 frames per second, with a pixel resolution of 800 x 600, capturing an observation window measuring 26.4 cm x 19.8 cm. As a result, 1 pixel equates to 0.033 cm in physical space. Due to constraints posed by the aluminum frame, the initial launch point is not captured, with the first recorded vertical coordinate of the particle's center of mass approximated at $Y_{CM} \simeq 16$ cm. ImageJ software [26] is used to analyze images (see examples in Figs. 3 and 4), determining the positions of the particle's center of mass and the small orifice near the border, which allows tracking rotations. In Figs. 3 and 4, we present snapshots images for a $N = 3$ faceted particle and a disk

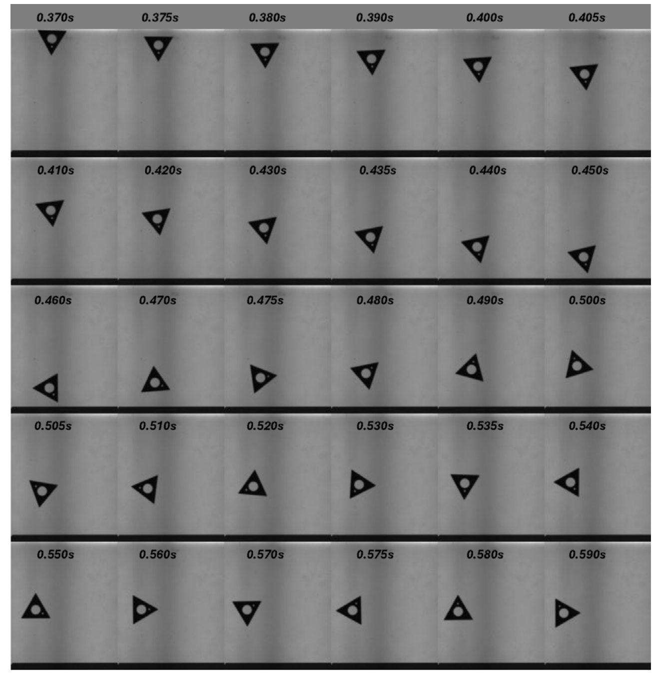

Fig. 3. Snapshots images for $N = 3$ faceted particle. Collision takes place between times 0.46 s and 0.47 s.

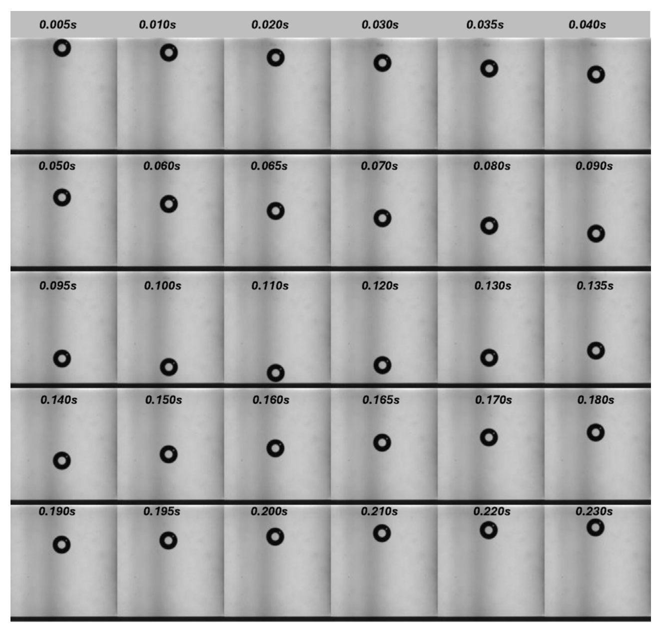

Fig. 4. Snapshots images for $N = \infty$ faceted particle, i.e. disk. Collision takes place between times 0.41 s and 0.42 s.

($N = \infty$), respectively. For $N = 3$, rotations and lateral displacements are clearly observed after collision (Fig. 3). In contrast, for the disk (Fig. 44), post-collision motion is perpendicular to the impact surface, with negligible lateral motions and rotations.

As already mentioned, this image processing enables trajectory measurements (some examples can be found in [24]) and the extraction of translational and rotational velocities. A discernible shift in vertical velocity sign occurs upon collision with the flat surface, allowing for the determination of V_n and V_n' from the local minima and maxima of the vertical velocity evolution, as detailed in previous research [24]. Given the sampling rate and the ability to detect a minimum displacement of 1 pixel, velocities below 13 cm/s cannot be accurately measured and are thus filtered from the data. Typically, the particle rebounds between 3 and 10 times until its velocity drops below a critical threshold of 13 cm/s. For each rebound, the coefficient of restitution, ϵ, is computed using V_n and V_n' (as per Eq. (1)), derived from translational velocities of the particle's geometric center before and after impact, respectively. Considering particle size and a threshold value of 200 used in image analysis, positional coordinates are obtained with uncertainties of 0.1 pixels [27], resulting in velocity errors of $\Delta V = 2.6$ cm/s and relative errors $\Delta\epsilon/\epsilon \in [0.03, 0.19]$. For $\epsilon \leq 1$, the error $\Delta\epsilon$ ranges from 0.02 to 0.19, while for $\epsilon > 1$, the error $\Delta\epsilon$ varies from 0.04 to 0.33. Additionally, potential, translational kinetic, and rotational kinetic energies are calculated and analyzed during the relaxation process. It is noted that in subsequent rebounds, beyond the initial one, the impacting face of the particle cannot be controlled, yet it is assumed that significant alterations to the results would not arise from controlling the launch angle of the face.

This data allows to:

- Obtain the coefficient of restitution (Eq. (1)).
- Analyze the energy transfer between the different degrees of freedom: rotational and translational (parallel and transverse to gravity).
- Identify other possible coefficients to characterize the transfer/loss of energy in an impact.

At each sampling time n (i.e. each image), the rotational kinetic energy $E_{Rn} = \frac{I\omega_n^2}{2}$ was obtained. The angular velocity ω_n was calculated as $\omega_n = \frac{\theta_{n+1}-\theta_n}{\Delta t}$, where Δt the inverse of the sampling rate (1/391 s). Each θ represents the angle between the horizontal direction (perpendicular to gravity) and the segment defined by the position of the small orifice near the edge of each particle and the particle's center of mass. Eq. (3) was derived to obtain the moment of inertia I for each faceted particle, considering the centered perforation of radius r, which allows the detection of its center of mass.

$$I_{CM}(N) = \left\{ \left[\left[\frac{1}{8\,\sin^2\left(\frac{\pi}{N}\right)} - \frac{1}{12} \right] - \frac{2\,\pi\,r^4}{N\,a^4}\,tg\left(\frac{\pi}{N}\right) \right\} \times \frac{m\,N\,a^4}{N\,a^2 - 4\,tg\left(\frac{\pi}{N}\right)\pi\,r^2} \tag{3}$$

where a is the size of sides for a N faceted particle.

$$a(N) = R_N\sqrt{\frac{4\pi}{N}tg\left(\frac{\pi}{N}\right)} \tag{4}$$

Eqs. (3) and (4) condense in Eq. (5) which, for the disk, leads to $I_{CM} = m(R_\infty^2 + r^2)/2$ for N tending to ∞ (see Table 1 for values of R_N).

$$I_{CM}(N) = \left\{ \left[\left[\frac{\pi\,R_N^2}{2N\,\sin\left(\frac{\pi}{N}\right)\cos\left(\frac{\pi}{N}\right)} - \frac{\pi\,R_N^2}{3N}\,tg\left(\frac{\pi}{N}\right) \right] - \frac{r^4}{2R_N^2} \right\} \frac{m\,R_N^2}{R_N^2 - r^2} \tag{5}$$

Fig. 5 shows values of I_{CM}/I_{CM}^{DISK} as a function of $1/N$, i.e. for the disk $1/N = 0$. The moment of inertia I_{CM} slightly decreases with increasing N. For $N > 4$, the relative difference in I_{CM} compared to the disk ($I_{CM}^{DISK} = (3.81 \pm 0.41)$ g cm^2) is less than 2%. The largest difference in the value of I_{CM} compared to I_{CM}^{DISK} was observed for $N = 3$, with a relative difference of less than 22%.

Also, to evaluate the potential influence of interactions between the particle and the cell walls, we conducted tests by tilting the cell ±5° from the vertical to induce contact between the particle and the glass. We found no significant differences compared to the case with the cell in the vertical position.

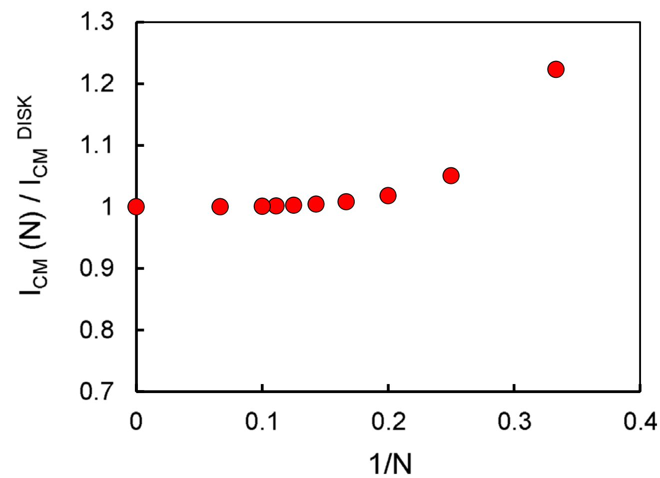

Fig. 5. Moment of inertia I_{CM} with respect of the center of mass (CM) as function of $1/N$, i.e. $1/N = 0$ corresponds to the moment of inertia of the disk including the centered hole of radio r.

Table 2
Number of collisions analyzed and number of collisions with $\epsilon > 1$ for each type of faceted particle.

N	# collisions	# and % collision with $\epsilon > 1$
3	1380	271 (19,6%)
4	304	52 (17,1%)
5	442	101 (22,8%)
6	383	88 (22,8%)
7	342	56 (16,4%)
8	344	52 (15,1%)
9	1497	175 (11,7%)
10	359	27 (7,5%)
15	349	1 (0,3%)
∞	516	0 (0%)

3. Experimental results

In this section, we report experimental results for collisions of the N- faceted particles. The number of collisions varies from 304 to 1380, details are given in Table 2.

3.1. Coefficient of restitution

Energy dissipation during each collision is quantified by ϵ, the coefficient of restitution (as per Eq. (1)), which does not considerate any effects resulting from rotations. Fig. 6 illustrates the results for ϵ plotted against the normal impact velocity for both the disk and triangular ($N = 3$) faceted particle.

Consistent with findings in previous studies [11–13], we observed that the dispersion of ϵ around its mean value (as depicted in Fig. 7) increases as the impact velocity decreases (refer to Fig. 8). Notably, the dispersion is appreciably greater for the faceted particle, and for low V_n values, the distribution of ϵ is asymmetric around each mean value. In Section 3.2 we will propose an explanation in terms of energy transfer.

It is noteworthy that for the triangular faceted particle, ϵ can exceed 1 at low impact velocities (bottom panel in Fig. 6). In fact, for $N = 3$, approximately 20% of collisions exhibited $\epsilon > 1$. This phenomenon was also observed for all faceted particles except the disk (refer to Table 2) and may be comprehended in terms of energy stored at impact, in alternative degrees of freedom, which is subsequently transferred in another collision to kinetic energy, resulting in an increase in V_n', the normal velocity after impact. The augmentation of energy in certain degrees of freedom upon impact and its subsequent release during another collision will be elucidated in the subsequent subsection.

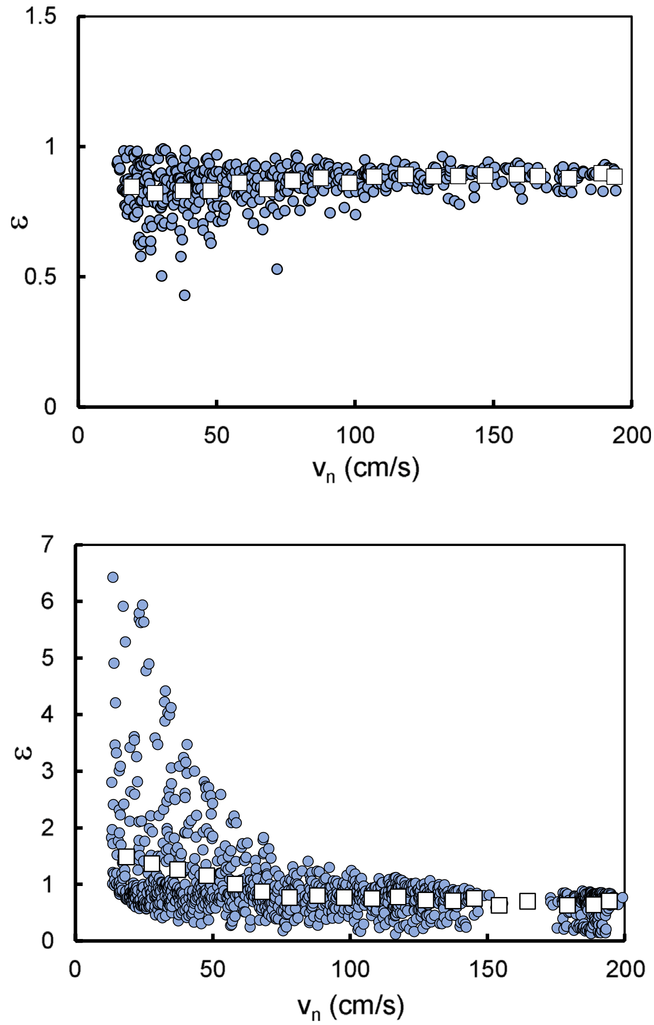

Fig. 6. Coefficient of restitution as a function of V_n, the vertical impact velocity for a particle colliding with a flat surface. Square markers indicate the mean values of ϵ, sampled within 10 cm/s windows for V_n, plotted against the average value $\langle V_n \rangle$ obtained within these windows. Top panel: ϵ values obtained for disk. Bottom panel: ϵ values obtained for $N = 3$ faceted particle.

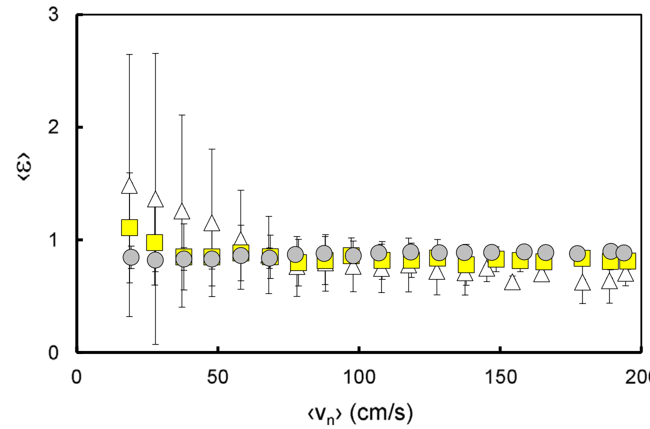

Fig. 7. Mean values $\langle \epsilon \rangle$ obtained in windows of width 10 cm/s of V_n. Empty triangles corresponds to $N = 3$ faceted particle, yellow squares corresponds to $N = 9$ faceted particle, and gray circles corresponds to disks. Magnitudes are plotted vs. mean values $\langle V_n \rangle$ obtained in the mentioned windows. Errors bars correspond to standard deviations σ obtained in windows of width 10 cm/s.

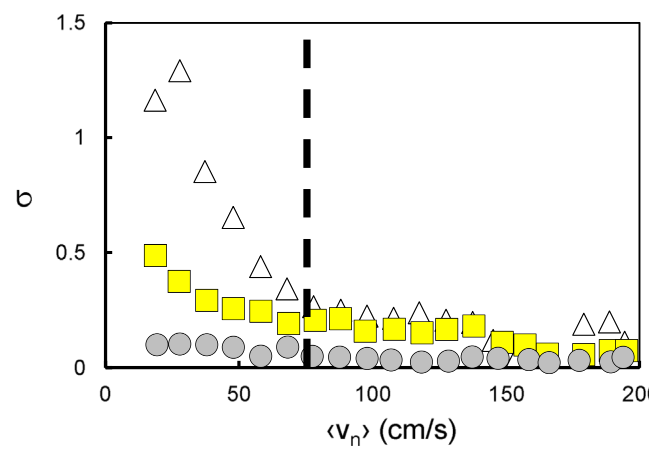

Fig. 8. Standard deviation σ obtained, for ϵ values, in windows of width 10 cm/s of $\langle V_n \rangle$. Empty triangles corresponds to $N = 3$ faceted particle, yellow squares corresponds to $N = 9$ faceted particle, and gray circles corresponds to disks. σ is plotted vs. mean values $\langle V_n \rangle$ obtained in the mentioned windows. Dashed line indicated the position of V_{n_o}.

In Fig. 7, we present mean values of ϵ, accompanied by uncertainty bars estimated from their standard deviations, plotted against mean values of $\langle V_n \rangle$. Both $\langle \epsilon \rangle$ and $\langle V_n \rangle$ are computed for samples obtained within windows of width 10 cm/s for $\langle V_n \rangle$.

It is observed that $\langle \epsilon \rangle$ decreases as $\langle V_n \rangle$ increases and for $V_{n_o} = (75 \pm 5)$ cm/s, $\langle \epsilon \rangle$ changes its behavior depending on the number of faces N.

On the one hand, for $\langle V_n \rangle \leq V_{n_o}$, as $\langle V_n \rangle$ decreases, faceted particles present less dissipation leading to collisions with $\langle \epsilon \rangle$ values that are not only larger than those obtained for the disk but might also reach values larger than 1. As N decreases, $\langle \epsilon \rangle$ increases and, for triangular particles, i.e. smallest N, the highest $\langle \epsilon \rangle$ values are registered.

On the other hand, for $\langle V_n \rangle > V_{n_o}$, the contrary is observed, the disk dissipated less energy in collisions leading to values of $\langle \epsilon \rangle$ that are larger than those obtained for the other studied faceted particles ($N \leq 15$). Fig. 8 shows that σ, the dispersion in ϵ values, decreases as the impact velocity V_n increases and reaches, at V_{n_o}, a constant value that depends on the number N of faces of the particle. Also, it can be observed that for a given value of V_n, the dispersion σ increases with N.

In Table 3 we present mean values $\langle \epsilon \rangle$ calculated with the average of mean values obtained in the following three conditions of impact velocities: $V_n > V_{n_o}$, i.e. high velocities; $V_n \leq V_{n_o}$, i.e. low velocities; and for the whole range of impact velocities V_n. For $N \leq 15$, the N-faceted particles can reach, at low velocities, mean values $\langle \epsilon \rangle > 1$.

Table 3
Mean value of the coefficient of restitution $\langle \epsilon \rangle$ calculated with the average of mean values obtained for the whole range of V_n and for $V_n > V_{n_o}$, i.e. high velocities and $V_n \leq V_{n_o}$, i.e. low velocities, being $V_{n_o} = 75$ cm/s.

V_n(cm/s)	N=3	N=9	$N = \infty$ (Disk)
0 − 200	0.86 ± 0.39	0.85 ± 0.14	0.87 ± 0.05
0 − 75	1.19 ± 0.79	0.92 ± 0.31	0.84 ± 0.09
75 − 200	0.72 ± 0.19	0.82 ± 0.13	0.88 ± 0.04

We also examined the behavior of the coefficient of restitution ϵ_E (as per Eq. (2)), which accounts for the overall energy loss during a collision. Unlike ϵ, this coefficient considers not only variations in translational kinetic energy associated with the particle's vertical motion but also accounts for changes in translational kinetic energy related to lateral displacements and alterations in rotational kinetic energy. As expected, ϵ_E consistently remains below 1. However, akin to observations for ϵ, it exhibits a wider dispersion at lower impact velocities, as illustrated in Fig. 9. Additionally, akin to $\langle \epsilon \rangle$ trends,

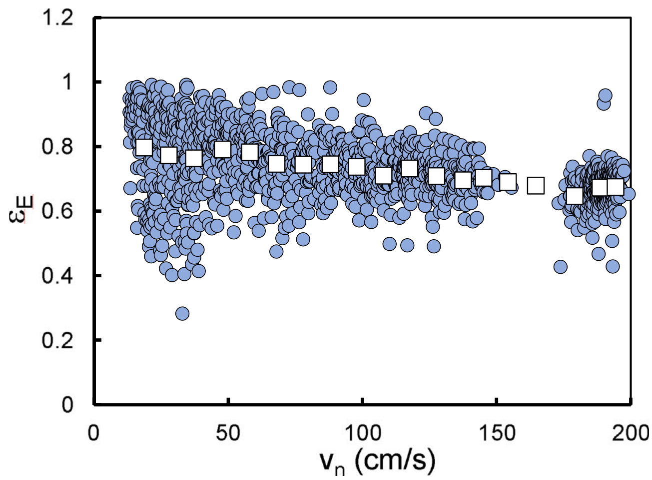

Fig. 9. Coefficient of restitution ϵ_E as a function of V_n, the vertical impact velocity for a $N = 3$ faceted particle colliding with a flat surface. Square markers are mean values of ϵ sampled in windows of width 10 cm/s for V_n, plotted vs. $\langle V_n \rangle$ obtained in the mentioned windows.

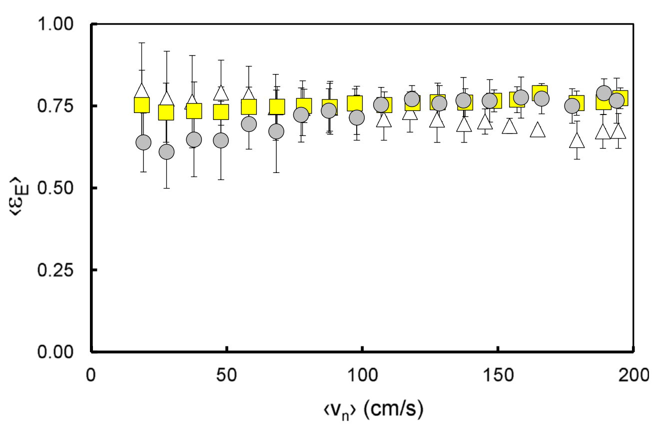

Fig. 10. Mean values $\langle \epsilon_E \rangle$ obtained in windows of width 10 cm/s of V_n. Empty triangles corresponds to $N = 3$ faceted particle, yellow squares corresponds to $N = 9$ faceted particle, and gray circles corresponds to disks. Magnitudes are plotted vs. mean values $\langle V_n \rangle$ obtained in the mentioned windows. Errors bars correspond to standard deviations σ obtained in windows of width 10 cm/s.

Table 4
Mean value of the coefficient of restitution $\langle \epsilon_E \rangle$ computed with the average of all values obtained for the whole range of V_n and for $V_n > V_{n_o}$, i.e. high velocities and $V_n \leq V_{n_o}$, i.e. low velocities, being $V_{n_o} = 75$ cm/s.

V_n(cm/s)	N=3	N=9	$N = \infty$ (Disk)
$0-200$	0.76 ± 0.05	0.76 ± 0.05	0.72 ± 0.07
$0-75$	0.74 ± 0.08	0.74 ± 0.08	0.65 ± 0.11
$75-200$	0.76 ± 0.04	0.76 ± 0.04	0.76 ± 0.06

$\langle \epsilon_E \rangle$ decreases with increasing V_n, and for $V_{n_o} = (75 \pm 5)$ cm/s, its behavior varies depending on the number of faces N. Consequently, for $\langle V_n \rangle \leq V_{n_o}$, as $\langle V_n \rangle$ diminishes, particles with fewer facets demonstrate lesser dissipation compared to those with more facets, such as the disk. Conversely, for $\langle V_n \rangle > V_{n_o}$, the disk dissipates less energy in the collision, resulting in $\langle \epsilon_E \rangle$ values surpassing those obtained for faceted particles with $N \leq 15$.

Fig. 10 displays the mean values $\langle \epsilon_E \rangle$ and their corresponding standard deviations σ, computed within 10 cm/s windows for $\langle V_n \rangle$. Notably, it is evident that the dispersion of $\langle \epsilon_E \rangle$ is more pronounced at lower velocities compared to higher velocities, yet for all particles, ϵ_E remains below 1.

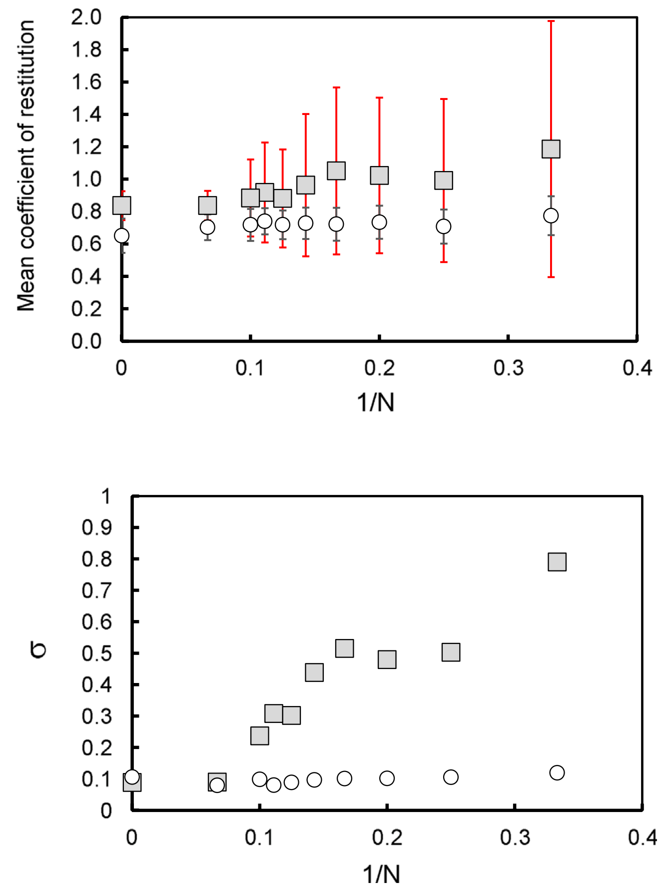

Fig. 11. Mean values of $\langle \epsilon \rangle$ (gray square) and $\langle \epsilon_E \rangle$ (empty circle) and its dispersion σ obtained for low impact velocities values, i.e. $V_n \leq V_{n_o}$, for $N = 3, 4, 5, 6, 7, 8, 9, 10, 15$ and ∞ (disk). Top panel: Mean values of $\langle \epsilon \rangle$ and $\langle \epsilon_E \rangle$, error bars are standard deviation σ (red for ϵ and black for ϵ_E). Bottom panel: σ for $\langle \epsilon \rangle$ (gray square) and $\langle \epsilon_E \rangle$ (empty square).

Also, mean values of $\langle \epsilon \rangle$ and $\langle \epsilon_E \rangle$ were calculated with the average of mean values obtained for high velocities ($V_n > V_{n_o}$) and low velocities ($V_n \leq V_{n_o}$).

In Table 4 we present mean values of $\langle \epsilon_E \rangle$ calculated with the average of mean values obtained when the impact velocity $V_n > V_{n_o}$, i.e. high velocities, $V_n \leq V_{n_o}$, i.e. low velocities, and for the whole range of impact velocities V_n.

For all the particles, ϵ_E remains below 1, resulting in mean values of $\langle \epsilon_E \rangle < 1$, and its dispersion is comparatively smaller than that of the coefficient of restitution ϵ. Fig. 11 illustrates mean values and standard deviations σ of $\langle \epsilon_E \rangle$ and $\langle \epsilon \rangle$ obtained for low impact velocities ($V_n \leq V_{n_o}$), while Fig. 12 depicts the same for high impact velocities ($V_n > V_{n_o}$).

At low impact velocities, the mean value of $\langle \epsilon_E \rangle$ and σ remains relatively constant for all N-faceted particles, whereas the mean values of $\langle \epsilon \rangle$ and its dispersion σ increase as N decreases.

Notably, similar results are observed for all magnitudes when $N = 15$ and for the disk. At high impact velocities, the mean value of $\langle \epsilon_E \rangle$ is slightly lower than $\langle \epsilon \rangle$ for $N \geq 10$, while for $N \leq 9$, they align within error bars. Also, in this case, for all N-faceted particle σ remains nearly constant for mean values of $\langle \epsilon_E \rangle$, whereas mean values of $\langle \epsilon \rangle$ increase as N decreases, albeit still smaller than those for low velocities. It is noteworthy that under these conditions, σ values are alike for $N = 15$ and the disk.

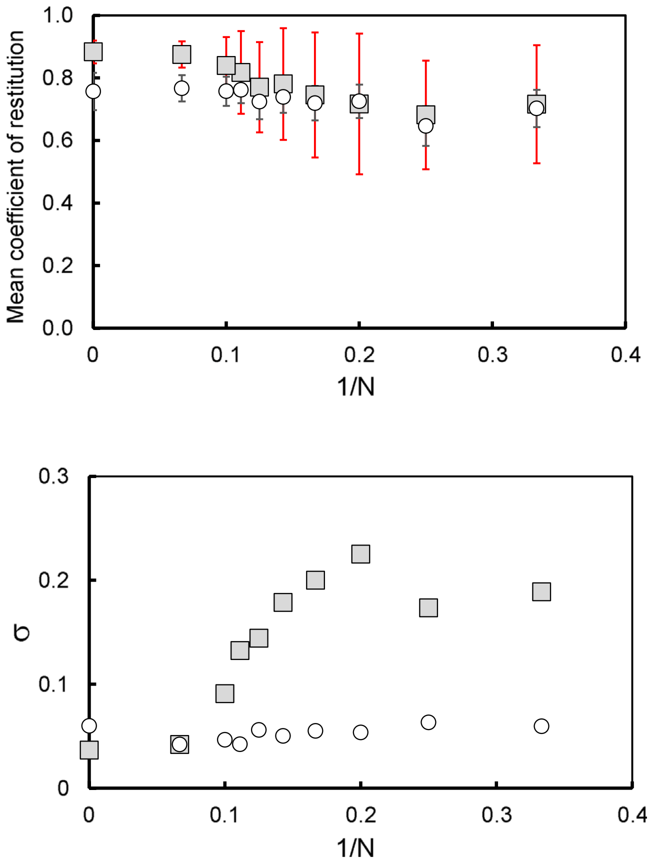

Fig. 12. Mean values of $\langle \epsilon \rangle$ (gray square) and $\langle \epsilon_E \rangle$ (empty circle) and its dispersion σ obtained for high impact velocities values, i.e. $V_n > V_{n_o}$, for $N = 3, 4, 5, 6, 7, 8, 9, 10, 15$ and ∞ (disk). Top panel: Mean values of $\langle \epsilon \rangle$ and $\langle \epsilon_E \rangle$, error bars are standard deviation σ (red for ϵ and black for ϵ_E). Bottom panel: σ for $\langle \epsilon \rangle$ (gray square) and $\langle \epsilon_E \rangle$ (empty circle).

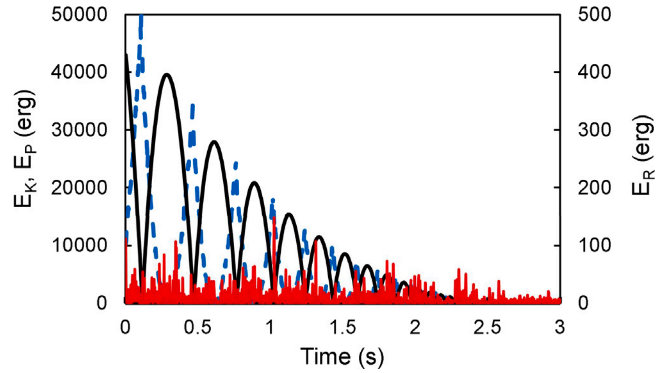

Fig. 13. Example of energy evolution during the relaxation process of a disk ($N = \infty$): translational kinetic energy (blue dashed line), rotational kinetic energy (red solid line) and potential energy (black line).

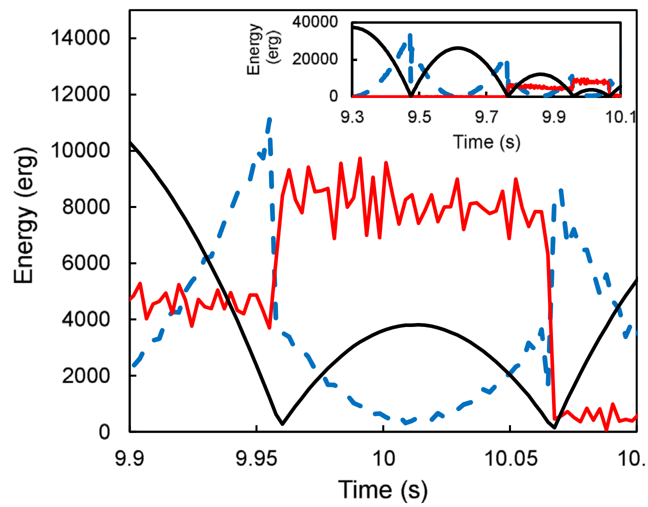

Fig. 14. Example of energy evolution during the relaxation process of a faceted particle ($N = 9$): translational kinetic energy (blue dashed line), rotational kinetic energy (red solid line) and potential energy (black line). Main panel: detail of inset panel for t = 9.9 s to t = 10.1 s, it can be observed that a first collision induces a rotation, translational kinetic energy is transfer to the rotational kinetic energy where it is stored until it is released in the next collision. Inset panel: extended example of the relaxation process for a faceted particle.

3.2. Energy transfer throughout the relaxation process

Initially, a particle is released from a height H_o with zero velocity and no spin. During its descent, the particle (whether a disk or a faceted particle) moves exclusively in the vertical direction and remains non-rotational. Upon colliding with the flat surface, the disk and the faceted particle exhibit distinct behaviors:

- Disk: considering that the disk has an uniform mass distribution and that the center of mass and the point of impact are aligned with the direction of gravity (vertical) no torques appear in the collision. Therefore, there is negligible rotational kinetic energy (E_R) throughout the relaxation process and translational kinetic energy only accounts for motion in the vertical direction ($E_K(V_y)$). An illustrative example is depicted in Fig. 13.
- Faceted particles: when a vertex of a faceted particle collides with the flat surface and the point of impact does not align with the center of mass in the vertical direction, it may induce torque, resulting in rotations and/or lateral displacement. Evidence of this phenomenon is presented in prior research [24]. Consequently, rotational kinetic energy (E_R) may increase due to impact and then, between successive collisions, E_R remains constant. For faceted particles, translational kinetic energy (E_K) accounts for motion in both, horizontal and vertical, directions ($E_K(V_x, V_y)$). In subsequent collisions, $E_K(V_x)$ (for transverse motion) and E_R previously gained may be either dissipated upon impact or partially transferred to $E_K(V_y)$ linked to vertical motion, leading to an increase in V_n'. Inset panel of Fig. 14 provides an illustrative example of the relaxation process for a faceted particle while the main panel highlights a detail where an initial collision induces rotation, with translational kinetic energy transferred to rotational kinetic energy and stored until it is released in the subsequent collision.

It is important to note that during collisions, energy variations may occur solely for $E_K(V_y)$, $E_K(V_x)$ and E_R. However, in experimental settings, due to the sampling rate in images acquisition, particles achieve different height values before and after a collision, resulting in spurious variations in potential energy i.e. $\Delta E_P \neq 0$, which lack physical significance. Hence, variations in E_P will not be analyzed.

Values of ϵ were determined solely using V_y' and V_y, i.e. V_n' and V_n in Eq. (1), hence collisions with $\epsilon > 1$, i.e. $V_n' > V_n$, indicate an increase in translational kinetic energy associated with the vertical motion ($\Delta E_K(V_y) > 0$). These increments should be related either to energy loss or to energy transfer from E_R and/or exchanges $E_K(V_x)$ to $E_K(V_y)$, i.e., $\Delta E_R < 0$ and/or $\Delta E_K(V_x) < 0$. Therefore, to comprehend the energy transfers resulting in collisions with $\epsilon > 1$ (refer to 2), the following negative energy transfer rates were obtained and analyzed: $\frac{\Delta E_K(V_y)}{\Delta E_R}$ and $\frac{\Delta E_K(V_y)}{\Delta E_K(V_x)}$. An illustrative example of collisions with $\epsilon > 1$

and negative energy transfer rates is depicted in Fig. 15 for $N = 9$. We observed the following:

- $\left|\frac{\Delta E_K(V_y)}{\Delta E_R}\right| \leq 1$ for most collisions (98%), i.e. $\Delta E_K(V_y) \leq |\Delta E_R|$, which indicates that an increase in $E_K(V_y)$, i.e. $\epsilon > 1$, could be explained with energy being transfer only from E_R.
- $\left|\frac{\Delta E_K(V_y)}{\Delta E_K(V_x)}\right| \leq 1$ for few collisions (7,5%, see Inset in the bottom of Fig. 15), i.e. $\Delta E_K(V_y) \leq |\Delta E_K(V_x)|$, and therefore the increase in $E_K(V_y)$ could be explained with energy being transfer only from $E_K(V_x)$. In the other collisions (92,5%) an increase in $E_K(V_y)$ needs to account for energy being transfer from other degrees of freedom besides from $E_K(V_x)$.

Considering only collisions with $\epsilon > 1$, Fig. 16 illustrates the percentage of collisions with negative energy transfer rates (where E_R and $E_K(V_x)$ decrease and $E_K(V_y)$ increase) that exhibit $|\frac{\Delta E_K(V_y)}{\Delta E_R}| \leq 1$ and $|\frac{\Delta E_K(V_y)}{\Delta E_K(V_x)}| \leq 1$. Only faceted particles with $N \leq 10$ present a sufficient number of collisions with $\epsilon > 1$ (refer to Table 2) to analyze these percentages. In fact, for disks, none of the collisions resulted in $\epsilon > 1$.

For faceted particles with $N \leq 10$, akin to the observation for $N = 9$ (Fig. 15), most collisions with $\epsilon > 1$ exhibit $\Delta E_K(V_y) \leq |\Delta E_R|$, indicating that an increase in $E_K(V_y)$, i.e. $\epsilon > 1$, can be attributed solely to energy transfer from E_R, with only a small percentage of collisions requiring energy transfer from lateral motion. Also, only a minor percentage of collisions can explain a notable increase in $E_K(V_y)$ only due to the transfer of $E_K(V_x)$. Therefore, most collisions require the transfer of E_R to $E_K(V_y)$, highlighting the importance of rotation in storing and releasing energy in subsequent collisions.

4. Conclusion

This experimental work analyses the role of rotation during collisions. Flat faceted particles were released in a Hele–Shaw cell to allow a quasi-two-dimensional translational motion and limited rotation around a single axis. Particles are faceted to promote the appearance of torques when particles collide over a flat surface leading to kinetic rotational energy being storage or transfer during the collision process.

The coefficient of restitution ϵ serves as a parameter to characterize the dissipation occurring in these collisions, determining the behavior of granular systems, albeit measured within constraints specified by Eq. (1).

Consistent with previous findings [11–13], ϵ is observed to depend on the impact velocity V_n, displaying a wider dispersion for lower impact velocities ($V_n < 75$ cm/s). The threshold value $V_{n_o} = 75$ cm/s, distinguishing low and high impact velocity regimes, may be associated with a deformation threshold related to the particle material. At higher impact velocities, particles undergo greater deformation at the contact point, resulting in lower values of V_n' due to increased energy dissipation and inhibited rotations. These characteristics lead to smaller values of ϵ and its dispersion σ. Further investigation using particles of different materials, e.g. different Young modulus, is necessary to validate this hypothesis.

Additionally, we analyzed energy transfer during collisions, providing experimental evidence that rotations induced upon impact can store rotational kinetic energy until a subsequent collision, where a significant portion of this stored energy can be transferred to vertical motion, explaining ϵ values above 1. Furthermore, we demonstrate that for collisions with $\epsilon > 1$, the translational kinetic energy associated with normal motion is more likely to be gained from rotational kinetic energy stored in a previous collision than from the translational kinetic energy associated with the lateral motion of the particle, which also accompanies rotations.

We observed that for $N \geq 15$, the occurrence of collisions with $\epsilon > 1$ decreases, with the probability of such events becoming insignificant (see Table 2). Therefore, for $N \geq 15$ the N-faceted particles behave like disks, meaning torques are negligible when particles collide with the flat surface. We inferred that this occurs because the vertices are very close to each other, and during a collision, two consecutive vertices make contact with the flat surface, resulting in a vertical impact that does not induce torque, thereby preventing rotations.

Furthermore, the storage and transfer of kinetic energy related to rotations and lateral displacements can account for the significant dispersion of ϵ, particularly important at lower impact velocities and for smaller N values.

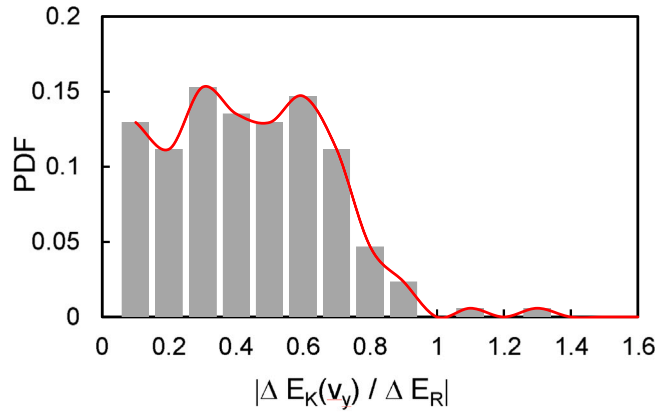

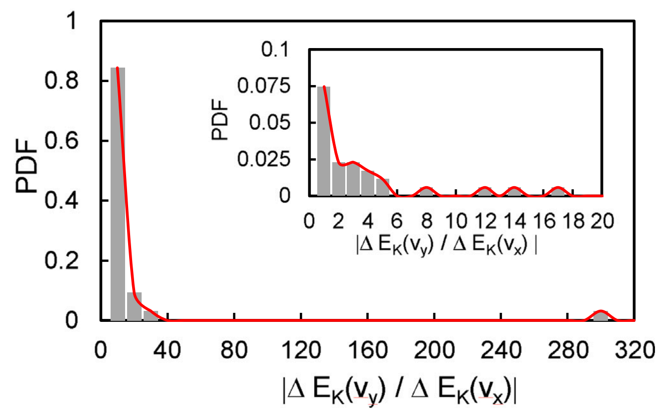

Fig. 15. Distributions of the modulus of energy transfer rates for collisions with $\epsilon > 1$ and negative energy transfer rates for the $N = 9$ faceted particle. Top panel- $\left|\frac{\Delta E_K(V_y)}{\Delta E_R}\right|$ ($Bin = 0.1$). Main bottom panel- $\left|\frac{\Delta E_K(V_y)}{\Delta E_K(V_x)}\right|$ ($Bin = 10$). Inset in bottom panel- $\left|\frac{\Delta E_K(V_y)}{\Delta E_K(V_x)}\right|$, detail with $bin = 1$. Red lines are to guide the eye.

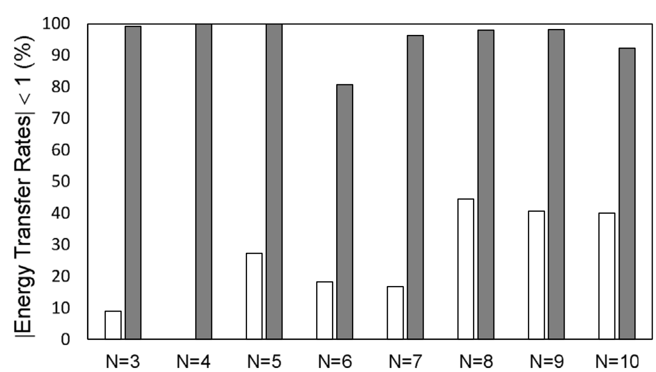

Fig. 16. Considering only collision with $\epsilon > 1$, figure presents the percentage of collisions with negative energy transfer rates and $|\frac{\Delta E_K(V_y)}{\Delta E_R}| \leq 1$ (gray bars), and $|\frac{\Delta E_K(V_y)}{\Delta E_K(V_x)}| \leq 1$ (white bars).

Therefore, we conclude that these features should be taken into consideration when assessing whether dissipation at impact should be characterized solely by ϵ, as defined in Eq. (1), or whenever possible, such as in two-dimensional systems, through measurements of ϵ_E.

CRediT authorship contribution statement

F.E. Fernández: Writing – original draft, Methodology, Investigation, Formal analysis, Data curation. **M.A. Aguirre:** Writing – original draft, Supervision, Software, Resources, Project administration, Methodology, Investigation, Funding acquisition, Formal analysis, Conceptualization. **R.G. Martino:** Writing – review & editing, Software, Methodology, Investigation, Formal analysis, Conceptualization. **A. Boschan:** Writing – review & editing, Resources, Methodology, Investigation, Formal analysis. **M.F. Piva:** Writing – review & editing, Supervision, Software, Resources, Methodology, Investigation, Funding acquisition, Formal analysis, Conceptualization.

Declaration of competing interest

The authors declare that they have no known competing financial interests or personal relationships that could have appeared to influence the work reported in this paper.

Data availability

Data will be made available on request.

Acknowledgments

This work has been supported by the ANPCyT (Argentina) through Grant No. PICT-2014-2587 and by the Centro Argentino Francés de Ciencias de la Ingeniería (CAFCI, CONICET-CNRS) through Grant No. R147-15. We would like to express our gratitude to Marcos Madrid, Pablo Cobelli, and Pablo Balenzuela for their valuable comments and suggestions. Additionally, we appreciate the graphic design advice provided by María Verónica Aguirre.

References

[1] M. Piva, R.G. Martino, J.-C. Géminard, M.A. Aguirre, Phys. Rev. E 98 (2018) 062902.
[2] R. Fischer, P. Gondret, B. Perrin, M. Rabaud, Phys. Rev. E 78 (2008) 021302.
[3] C.J. Olson, C. Reichhardt, M. McCloskey, R.J. Zieve, Europhys. Lett. 57 (2002) 904.
[4] F. Cantelaube, Y. Limon-Duparcmeur, D. Bideau, G.H. Ristow, J. Phys. (France) I 5 (1995) 581.
[5] S.G.W. Williams, D.J. Furbish, Earth Surf. Dynam. 9 (2021) 701–721.
[6] D.J. Furbish, S.G.W. Williams, D.L. Roth, T.H. Doane, J.J. Roering, ESurf 9 (3) (2021) 577–613.
[7] R. Bharadwaj, C. Smith, B.C. Hancock, Int. J. Pharm. 402 (1–2) (2010) 50–56.
[8] C. Zhu, D. Wang, X. Xia, Z. Tao, M. He, C. Cao, Nat. Hazards Earth Syst. Sci. 18 (2018) 1811–1823.
[9] K. Rajaonarivony, X. Rouau, K. Lampoh, J.-Y. Delenne, C. Mayer-Laigle, Bioengineering 6 (2019) 102.
[10] J. Wang, C. Xu, Y. Xu, Z. Wang, X. Qi, J. Wang, W. Zhou, H. Tang, Q. Wang, Appl. Sci. 11 (2021) 5884.
[11] M. Montaine, M. Heckel, C. Kruelle, T. Schwager, T. Pöschel, Phys. Rev. E 84 (2011) 041306.
[12] H. King, R. White, I. Maxwell, N. Menon, Europhys. Lett. 93 (2011) 14002.
[13] R. Sondergaard, K. Chaney, C.E. Brennen, J. Appl. Mech. 57 (1990) 694.
[14] P. Gondret, M. Lance, L. Petit, Phys. Fluids 14 (2002) 643.
[15] Z. Jiang, J. Du, C. Rieck, A. Bück, E. Tsotsas, Powder Technol. 360 (2020) 352–365.
[16] X. Li, M. Dong, D. Jiang, S. Li, Y. Shang, Powder Technol. 362 (2019) 17.
[17] L. Cai, S. Wang, Y. Li, J. Mao, F. Li, Z. Liu, J. Gao, Powder Technol. 381 (2021) 110.
[18] J. Wang, H. Yang, L. Feng, M. Zhang, Y. Wu, G. Yue, Powder Technol. 366 (2020) 137–143.
[19] I. Yardeny, D. Portnikov, H. Kalmana, Adv. Powder Technol. 31 (9) (2020) 3747–3759.
[20] Thorsten Pöschel, Thomas Schwager, Computational Granular Dynamics: Models and Algorithms, Springer, 2005.
[21] T. Schwager, T. Pöschel, Granul. Matter 9 (2007) 465–469.
[22] E. Borsa, H.A. Petit, J. Piña, C.I. Paulo, E.F. Irassar, EPJ Web Conf. 249 (2021) 05006.
[23] M.V.C. Machado, R.M. Lima, R.J. Brandão, C.R. Duarte, M.A.S. Barrozo, Braz. J. Chem. Eng. 40 (2023) 177–191.
[24] F.E. Fernández, M. Piva, R.G. Martino, M.A. Aguirre, EPJ Web Conf. 249 (2021) 06007.
[25] V. Nagarajan, A.K. Mohanty, M. Misra, ACS Sustain. Chem. Eng. 4 (6) (2016) 2899–2916.
[26] C.A. Schneider, W.S. Rasband, K.W. Eliceiri, Nat. Methods 9 (2012) 671.
[27] Y. Feng, J. Goree, Bin Liu, Rev. Sci. Instrum. 78 (2007) 053704.